



Article

Effect of the Basicity on Mineralogical Phases and Micro-Structure of Dephosphorization Slag in the New Double Slag Converter Steelmaking Process

Wenkui Yang ¹, Jian Yang ^{1,*}, Runhao Zhang ¹, Han Sun ¹ and Yunlong Qiu ²

¹ State Key Laboratory of Advanced Special Steel, School of Materials Science and Engineering, Shanghai University, Shanghai 200444, China; yangwenkui@shu.edu.cn (W.Y.); zhangrunhao@shu.edu.cn (R.Z.); sun_han@shu.edu.cn (H.S.)

² Zhongxing Energy Equipment Co., Ltd., Haimen 226126, China; dongyh1115@zxnzyzb.com

* Correspondence: yang_jian@t.shu.edu.cn; Tel.: +86-21-6613-6580

Abstract: In the present work, the effect of the basicity at the lower range from 0.98 to 2.13 on dephosphorization of hot metal at 1623 K was studied through high-temperature laboratorial experiments. With the increase of the basicity from 0.98 to 2.13, the P and C contents in hot metal rapidly decrease and increase at first, and then gradually decrease and increase, respectively. From the scanning electron microscopy-energy dispersive X-ray spectroscopy (SEM-EDS) and X-ray diffraction (XRD) results, with the increase of the basicity, the phase containing the high P content changes from the matrix phase into the phosphorus (P)-rich phase. Under the present experimental conditions, the P-rich phase can only be precipitated from the liquid slag when the basicity is higher than 1.55, which is a benefit to the dephosphorization. As the Raman intensity of the P-O-Ca structure unit in the P-rich phase is significantly higher than that of the P-O-Si structure unit, most of the phosphorus in the P-rich phase exists in the P-O-Ca structure unit and a small amount of phosphorus exists in the P-O-Si structure unit. With the increase of the basicity of the dephosphorization slag, the activity coefficient of P_2O_5 , $\gamma_{(P_2O_5)}$, in the liquid phase decreases, while the basicity in the liquid phase increases.

Keywords: dephosphorization; low temperature; low basicity; mineralogical morphology; micro-structure



Citation: Yang, W.; Yang, J.; Zhang, R.; Sun, H.; Qiu, Y. Effect of the Basicity on Mineralogical Phases and Micro-Structure of Dephosphorization Slag in the New Double Slag Converter Steelmaking Process. *Metals* **2021**, *11*, 1480. <https://doi.org/10.3390/met11091480>

Academic Editors: Pasquale Cavaliere and Alexander McLean

Received: 21 July 2021

Accepted: 15 September 2021

Published: 17 September 2021

Publisher's Note: MDPI stays neutral with regard to jurisdictional claims in published maps and institutional affiliations.



Copyright: © 2021 by the authors. Licensee MDPI, Basel, Switzerland. This article is an open access article distributed under the terms and conditions of the Creative Commons Attribution (CC BY) license (<https://creativecommons.org/licenses/by/4.0/>).

1. Introduction

In the new double slag converter steelmaking process (NDSP), the dephosphorization and desiliconization are simultaneously conducted with a lower basicity slag at low temperature. Then the converter is tilted immediately for the deslagging as much as possible. The decarburization is subsequently performed in the same converter. After tapping, the decarburization slag with high basicity is left in the furnace for dephosphorization in the next heat. This process can significantly reduce the lime consumption and the amount of the slag emission [1].

The Ca_2SiO_4 (C_2S) can combine with the $Ca_3(PO_4)_2$ (C_3P) to form a $nCa_2SiO_4-Ca_3(PO_4)_2$ (nC_2S-C_3P) solid solution over a wide composition range at about 1673 K [2]. Since the dephosphorization slag used in the NDSP usually contains the saturated C_2S , it can combine with the C_3P in the liquid slag phase to form the nC_2S-C_3P solid solution to improve the dephosphorization ratio [3–7]. Therefore, the slag basicity determining the amount of the C_2S particles plays an important role in the NDSP.

There were some previous studies on the effect of basicity on the mineralogical phases of the dephosphorization slag [3,4,6,8–11]. For example, Lin et al. studied the effect of basicity on the mineralogical phases of $CaO-SiO_2-MgO-Al_2O_3-Fe_2O_3-P_2O_5$ slag by cooling the evenly melted slag to 1623 K. It was found that the crystal sizes of metal oxides (RO)

or spinel phases become smaller in higher basicity slag and the P content in the nC_2S-C_3P solid solution increased with the decrease of the basicity [9]. Shu et al. also reported that P_2O_5 content in the nC_2S-C_3P phase slightly decreases with the increase of the basicity due to the increase of C_2S content in the nC_2S-C_3P phase [8]. Uchida et al. reported that when basicity is larger than 0.8, the phosphorus (P)-rich phase is observed [10]. In our previous work [12] and in the previous works of Wang et al. [13,14], the investigation results of micro-structure of dephosphorization slag showed that P_2O_5 acts as an acidic oxide and has a stronger affinity with Ca^{2+} ions, resulting in the removal of Ca^{2+} ions from the Si-O-Ca linkage bond to form Si-O-Si and P-O-Ca linkages.

As stated above, the previous works about the effect of the basicity on mineralogical phases and micro-structure of dephosphorization slag in the NDSP at 1623 K are quite limited and need to be studied. In our previous works, the effects of the temperature, the initial P content in the hot metal, and the Fe_2O_3 addition amount on dephosphorization of hot metal in the NDSP have been studied [12,15,16]. Besides, the effect of the temperature on the micro-structure and viscosity of dephosphorization slag in the NDSP has also been investigated [17].

In the present work, the effect of the basicity on the mineralogical phases and micro-structure of dephosphorization slag with the lower slag basicity of 0.98~2.13 at 1623 K was studied through high-temperature laboratorial experiments for NDSP. The effect of the basicity on the removal ratios of Si, Mn, P, and C in hot metal was clarified. The influence of basicity on the micro-morphologies and mineralogical phases of dephosphorization slag was investigated using the scanning electron microscopy-energy dispersive X-ray spectroscopy (SEM-EDS) and X-ray diffraction (XRD) methods, respectively. Moreover, the micro-structures of the dephosphorization slag were analyzed with Raman spectroscopy, and the effect of slag basicity on the activity coefficient of P_2O_5 and the basicity of liquid slag were further studied.

2. Experimental Procedure

2.1. Preparation of Decarburization Slag and Pig Iron

Table 1 shows the target and actual compositions of the decarburization slag, whose mineralogical structures and chemical compositions are similar to those of the final slag in the industrial decarburization process. The detailed preparation process and mineralogical structures can be referred to in our previous papers [15,16]. In Table 1, the basicity (R) is the mass ratio of CaO to SiO_2 .

Table 1. Target and actual compositions of decarburization slag (mass%).

Sample	CaO	MgO	MnO	P_2O_5	SiO_2	FeO	R
Target	46.5	8.20	3.73	3.00	15.6	22.0	2.98
Actual	43.4	8.58	4.57	3.01	16.2	21.8	2.69

The mixtures of the pure iron blocks, graphite blocks, ferrophosphorus powders, silicon powders, and manganese powders were melted to prepare the pig irons in a vacuum induction furnace. The detailed preparation method can also be referred to in our previous paper [15].

2.2. Experimental Procedure and Analysis Method

In the present work, the same amounts of decarburization slag and iron ore were used and the same initial Si content in hot metal was maintained as far as possible. In addition, the appropriate amounts of lime powders were added to adjust the slag basicity to the predetermined values. In each experiment, about 300 g pig iron was placed into an alumina crucible and heated to 1623 K. Then, a small silica tube was used to remove the initial hot metal sample by suction. Subsequently, the mixtures of 18 g decarburization slag, 25 g Fe_2O_3 powders, and proper amounts of lime powders ranging from 0 to 9 g were added

immediately. According to the previous study by Xia et al. [18], the dephosphorization reaction could reach the quasi-equilibrium state when the reaction time of each experiment was 15 min. Therefore, the reaction time of each experiment was set to be 15 min. The detailed experimental procedure and experiment apparatus can be referred to in our previous papers [15,19].

When the reaction time reached 15 min, the alumina crucible was taken out from the electrical resistance furnace and quenched in water quickly. The embedded slag samples before carbon spraying were used for Raman analysis in the present work. The detailed analysis and characterization methods of the samples can be referred to in our previous paper [12].

The compositions of the initial hot metal and hot metal after dephosphorization are shown in Table 2. The compositions of oxides in the dephosphorization slag are shown in Table 3, in which each sample number corresponds to its slag basicity.

Table 2. Compositions of the initial hot metal and hot metal after dephosphorization (mass%).

Sample No.	[C] _i	[Si] _i	[Mn] _i	[P] _i	[C] _f	[Si] _f	[Mn] _f	[P] _f
R098	4.14	0.533	0.291	0.253	3.21	0.012	0.040	0.125
R117	4.16	0.587	0.310	0.282	3.61	0.017	0.051	0.104
R131	4.13	0.592	0.316	0.286	3.72	0.017	0.055	0.092
R155	4.15	0.731	0.263	0.311	3.89	0.017	0.064	0.095
R186	4.16	0.521	0.261	0.304	3.91	0.014	0.074	0.080
R213	4.21	0.494	0.310	0.273	3.97	0.014	0.101	0.061

Table 3. Compositions of oxides in the dephosphorization slag (mass%).

Sample No.	T.Fe	FeO	CaO	SiO ₂	Al ₂ O ₃	MgO	MnO	P ₂ O ₅	R
R098	26.0	32.8	20.7	21.2	10.41	3.98	5.14	4.17	0.98
R117	27.3	34.1	22.8	19.4	10.83	3.28	4.48	4.07	1.17
R131	23.6	29.3	26.0	19.9	12.1	3.28	4.45	4.7	1.31
R155	21.3	26.4	31.2	20.1	10.35	3.18	3.86	4.34	1.55
R186	21.8	27.1	33.9	18.2	8.79	3.26	3.44	4.80	1.86
R213	23.5	29.4	33.4	15.7	10.33	2.98	3.28	4.39	2.13

3. Results

3.1. Effect of Basicity on the Contents and Removal Ratios of Elements in the Hot Metal after Dephosphorization

Figure 1 shows the effect of basicity on the contents of elements in the hot metal after dephosphorization. With the increase of the basicity, the C and Mn contents in the hot metal increase gradually, the P content in the hot metal decreases, while the Si content in the hot metal is about 0.015% and changes little. When the basicity is 2.13, the P content reaches the lowest value of 0.061%. Figure 2 shows the effect of basicity on the removal ratios of the elements in the hot metal after dephosphorization. It can be seen that the removal ratios of elements correspond to the results in Figure 1.

According to the results of Zhu et al. [20], the equilibrium distribution ratio of Mn decreases with the increase of the basicity. Therefore, the removal ratio of Mn decreases with the increase of the basicity of dephosphorization slag gradually. With the increase of the basicity from 0.98 to 1.31, the P and C contents in hot metal rapidly decrease and increase at first, respectively. With the increase of the basicity from 1.31 to 2.13, the P and C contents gradually decrease and increase, respectively. It can be clearly seen that the oxidations of P and C are the competitive reactions. With the increase of the basicity, the oxidation of P is promoted, while the oxidation of carbon is inhibited. The other elements have some influence on the phosphorus removal, especially Si, because the affinity between Si and O is the strongest. Generally, after Si is removed from the hot metal, the phosphorus begins to be removed. According to our previous work [21], when the reaction time is

about 6 min, the Si content in the hot metal is decreased to a very low level. Therefore, when the reaction time is 15 min in the present experiments, the Si content in the hot metal should also be decreased to a very low level.

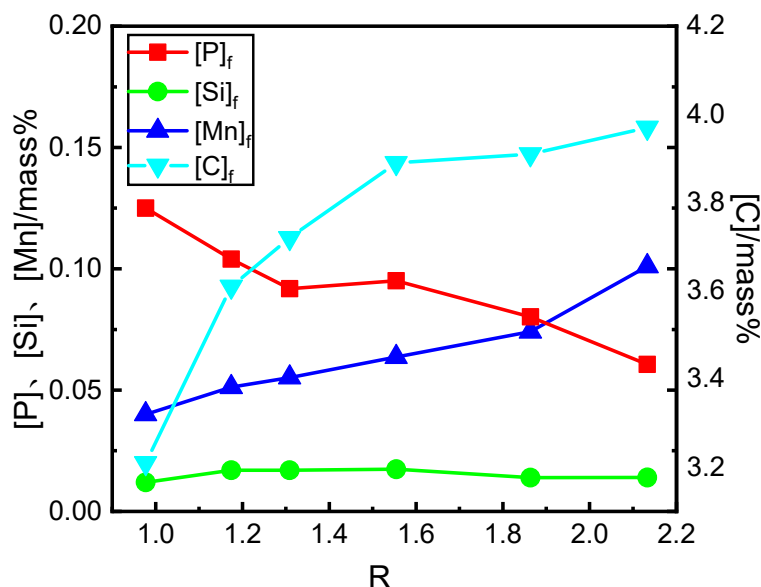


Figure 1. Effect of basicity on the contents of elements in the hot metal after dephosphorization.

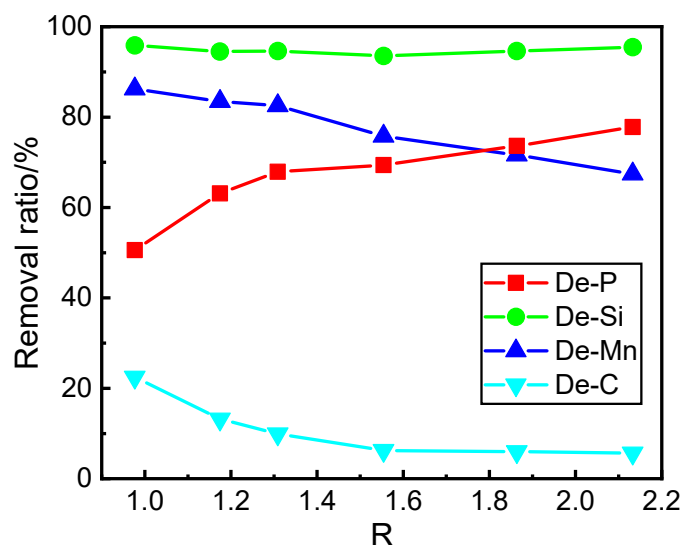


Figure 2. Effect of basicity on the removal ratios of the elements in the hot metal after dephosphorization.

3.2. Effect of Basicity on the Oxide Contents in Slag

Figure 3 shows the effect of basicity on the P_2O_5 , MnO, T.Fe, and Al_2O_3 contents in slag. With the increase of the basicity, the MnO content in slag decreases obviously, the P_2O_5 content increases slightly, the T.Fe content first decreases and then changes slightly, and the Al_2O_3 content changes little.

The change of MnO content in slag with basicity is basically consistent with the change of Mn content in the hot metal with basicity, as shown in Figure 1. Because different amounts of lime are added to adjust the basicity, the amounts of slag are increased with the increase of the basicity, which will lead to the decrease in the P_2O_5 content in slag. On the other hand, the promotion of dephosphorization increases the P_2O_5 content in slag with the increase of the basicity. As a result, the P_2O_5 content in slag only increases slightly with the increase of the basicity.

When the basicity is increased from 0.98 to 1.17, the T.Fe content in slag increases slightly. The removal ratio of C in hot metal with the basicity of 0.98 is much higher than that with the basicity of 1.17, which results in a larger amount of FeO consumed and a lower T.Fe content in slag. When the basicity is increased to 1.55, the T.Fe content in slag will decrease with the increase of the amount of slag. With further increasing of the basicity, because the total amount of FeO consumed by the oxidation reaction of each element in hot metal does not change much, the T.Fe content in slag changes slightly.

The Al_2O_3 content in slag depends on two factors. The erosion of alumina crucible will increase its content in slag, while the increase in the slag amount with the increase of the basicity will decrease its content in slag. Therefore, the Al_2O_3 content in slag changes slightly with the increase of the basicity.

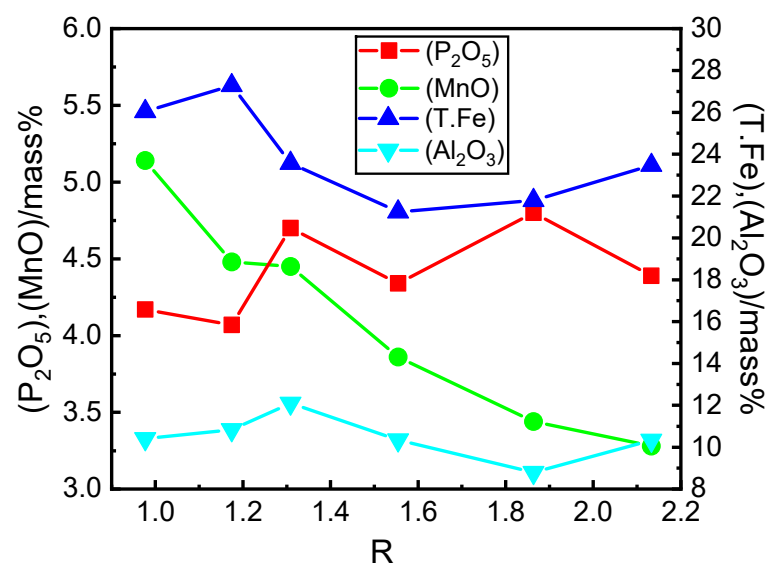


Figure 3. Effect of the basicity of the dephosphorization slag on the P_2O_5 , MnO, T.Fe, and Al_2O_3 contents in slag.

Since the main components in dephosphorization slag are CaO, SiO_2 , and FeO, and phosphorus-rich phase has the main components of CaO, SiO_2 , and P_2O_5 , Figure 4a,b show the compositions of dephosphorization slags located in CaO- SiO_2 -FeO ternary phase diagram and the compositions of the corresponding P-rich phases located in CaO- SiO_2 - P_2O_5 ternary phase diagram, respectively, at different basicities with the temperature of 1623 K, drawn with Factage7.3. The corresponding values of phosphate capacity, $C_{\text{PO}_4^{3-}}$, calculated in Equations (1) and (2) are also marked in Figure 4a [22]. In Figure 4a, when the basicity is lower than 1.31, the dephosphorization slags are located in the liquid phase region. When the basicity is increased to 1.31, the dephosphorization slag is located at the boundary between the C_2S -saturated region and the liquid phase region. When the basicity is in the range of 1.55~2.13, the dephosphorization slags are located in the C_2S -saturated region of the L + C_2S region. It can be seen from the table in Figure 4a that the phosphate capacity is gradually increased as the basicity is increased from 0.98 to 2.13. In Figure 4b, the compositions of all the P-rich phases located in the $n\text{C}_2\text{S}$ - C_3P -saturated region are close to the connection line between C_2S and C_3P in the phase diagram.

$$\log C_{\text{PO}_4^{3-}} = 0.0938[(\% \text{CaO}) + 0.5(\% \text{MgO}) + 0.3(\% \text{T.Fe}) + 0.35(\% \text{P}_2\text{O}_5) + 0.46(\% \text{MnO})] + 32500/T - 17.74 \quad (1)$$

$$\log C_{\text{PO}_4^{3-}} = \log C_{\text{PO}_4^{3-}} + 21680/T + 1.87 \quad (2)$$

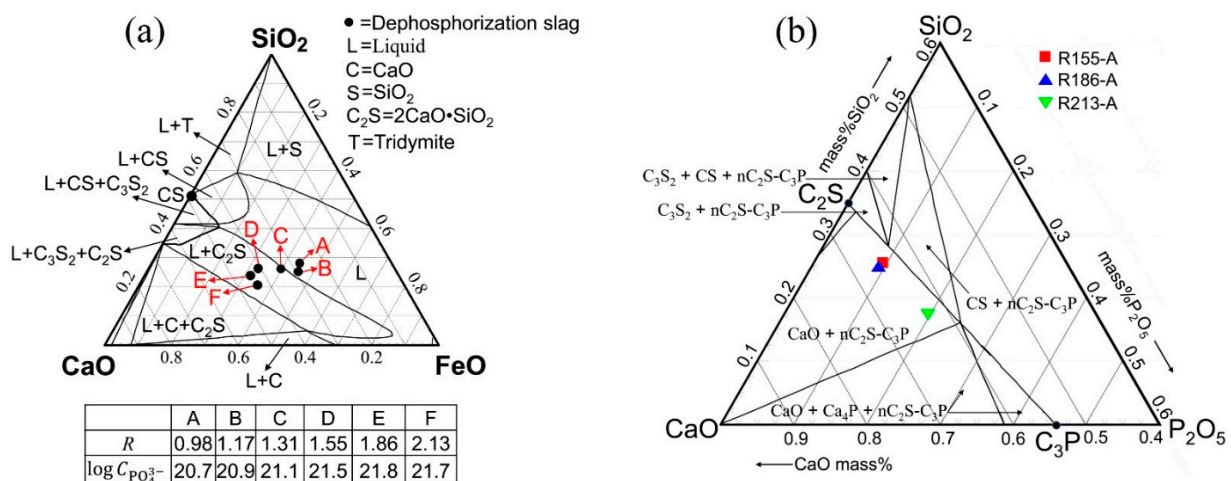


Figure 4. (a) Compositions of dephosphorization slags located in the CaO-SiO₂-FeO ternary phase diagram; (b) compositions of the corresponding P-rich phases located in the CaO-SiO₂-P₂O₅ ternary phase diagram.

4. Discussion

4.1. Influence of Basicity on the Micro-Morphologies of Dephosphorization Slag with SEM-EDS Analysis

Figures 5 and 6 show the SEM images of dephosphorization slag with magnification of 200 times and 1000 times at different basicities, respectively. Table 4 shows the corresponding compositions of each phase determined by EDS for dephosphorization slags with different basicities.

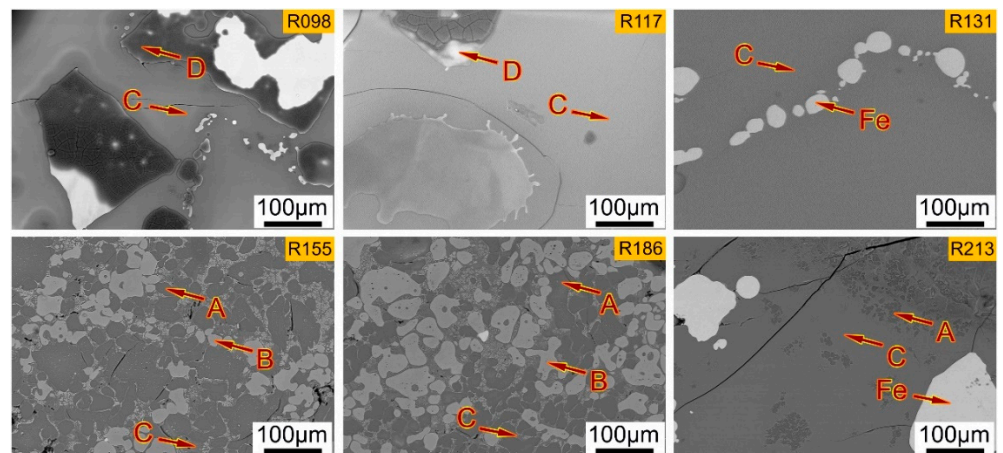


Figure 5. SEM images of dephosphorization slag with magnification of 200 times at different basicities.

Combining Figures 5 and 6, and Table 4, it can be seen that the phases in the slag of R098 and R117 are mainly composed of matrix phase C rich in P and Fe₂SiO₄ phase D. Besides, a small amount of spinel phase E rich in Al, Mg, Fe, and Mn was found in R098. However, the phases in slag of R131 are mainly composed of matrix phase C rich in P and a small amount of Fe phase containing pure iron.

It can be inferred that at low basicity, the FeO and SiO₂ in the molten slag will react to form Fe₂SiO₄. The reaction equation is shown in Equation (3). Because the melting point of Fe₂SiO₄ is 1493 K, Fe₂SiO₄ phase should not be precipitated in the molten slag at the actual dephosphorization temperature of 1623 K. Therefore, the Fe₂SiO₄ phase may be precipitated from the matrix phase when the crucible is taken out from the furnace to be quenched rapidly. Equation (4) is the Gibbs free energy equation of Equation (3). When the temperature is lower than 1716 K, ΔG⁰ is negative. This indicates that Equation (3) can

occur. In addition, the pure iron is found, as shown in the bright white phase near the D phase of Fe_2SiO_4 at R098 in Figure 5.



$$\Delta G^0 = -36200 + 21.09T \quad (4)$$

However, when the basicity is increased to 1.31, the SiO_2 content in slag decreases, which leads to the decrease in the corresponding SiO_2 content in the matrix phase, as shown in Table 4. Therefore, with the increase of the basicity, it is found that the D phase of Fe_2SiO_4 does not form after the quenching.

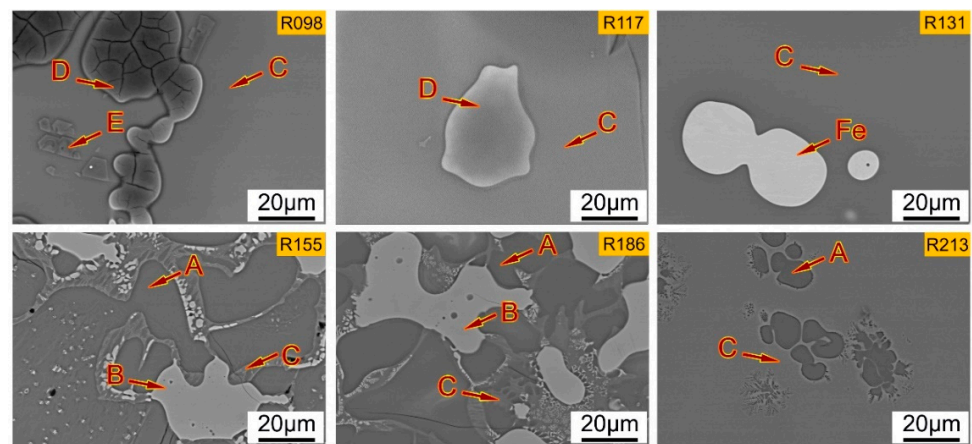


Figure 6. SEM images of the dephosphorization slag with magnification of 1000 times at different basicities.

Table 4. Compositions of each phase determined by EDS for dephosphorization slags with different basicities (mass%).

Position	MgO	Al_2O_3	SiO_2	P_2O_5	CaO	MnO	FeO
R098-D	0.15	0.11	47.1	0.18	0.31	0.11	52.0
R098-E	13.0	41.8	1.56	0.25	1.57	9.29	32.6
R098-C	3.74	8.61	24.6	6.46	30.4	7.00	19.2
R117-D	0.21	0.11	45.1	0.45	0.52	0.27	53.3
R117-C	3.01	10.3	24.6	5.66	32.1	6.13	18.1
R131-C	2.46	8.47	19.6	6.08	35.9	5.12	22.4
R155-A	0.86	0.11	24.1	8.48	61.4	1.45	3.64
R155-B	10.2	0.27	0.49	0.33	0.82	9.00	78.9
R155-C	1.39	8.59	21.38	0.97	45.6	2.98	19.1
R186-A	0.62	0.10	23.4	8.63	62.4	1.08	3.83
R186-B	10.8	0.34	0.02	0.43	0.60	10.0	77.8
R186-C	2.60	11.3	17.0	1.30	38.0	4.86	24.9
R213-A	0.58	0.34	16.8	18.9	60.1	1.05	2.19
R213-C	2.00	15.1	11.9	2.16	34.3	5.63	29.0

The slags of R155 and R186 are mainly composed of P-rich phase A, Fe-rich phase B, and matrix phase C. The black P-rich phase A contains high content of P_2O_5 in the form of $n\text{Ca}_2\text{S}-\text{C}_3\text{P}$ solid solution. The white Fe-rich phase B mainly contains FeO, MnO, and MgO. The matrix phase C is a liquid phase mainly containing CaO, SiO_2 , Al_2O_3 , FeO, MnO, and MgO.

The slag of R213 is mainly composed of P-rich phase A and matrix phase C. The P-rich phase A mainly exists in the form of small particles with the size less than 10 μm . Although the area fraction of P-rich phase A is less than those in slags of R155 and R186, the P_2O_5

contents in P-rich phase A and matrix phase C are much higher, so the dephosphorization ratio is higher.

From Table 4, it can be seen that the P content is high in the matrix phase C at the basicity of 0.98, 1.17, and 1.31, while the P content is high in the P-rich phase A at the basicity of 1.55, 1.86, and 2.13. Namely, with the increase of the basicity, the phase containing the high P content changes from the matrix phase C into the P-rich phase A. Therefore, under the present experimental conditions, the P-rich phase A can only be precipitated from the liquid slag when the basicity is higher than 1.55, which is a benefit to the dephosphorization.

4.2. Effect of Basicity on Mineralogical Phases of Dephosphorization Slag with XRD Analysis

Figure 7 shows the XRD diffraction patterns of the dephosphorization slag with different basicities. The phase compositions of dephosphorization slag are basically the same at the basicities of 0.98 and 1.17, which are mainly composed of metal oxide phase (RO), Fe_2SiO_4 , C_3P , and MgAl_2O_4 . When the basicity is increased to 1.31, the main phases in slag are C_3P and MgAl_2O_4 . This shows that when the basicity is lower than 1.31, the P in the slag mainly exists in the matrix phase in the form of C_3P . At the basicities of 0.98 and 1.17, the Fe_2SiO_4 is formed in the quenched dephosphorization slag, which is completely consistent with the results in Figure 6 and Table 4.

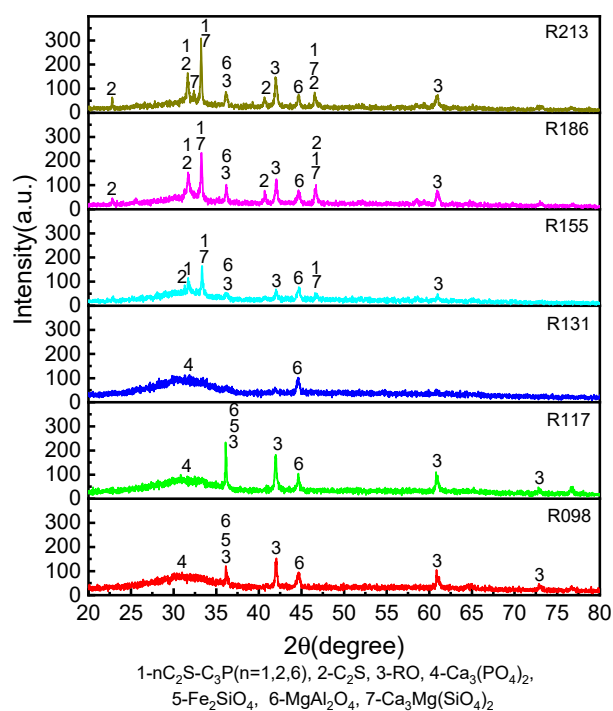


Figure 7. XRD patterns of the dephosphorization slag with different basicity.

As the basicity is increased from 1.55 to 2.13, the phase compositions of dephosphorization slags are basically the same, which mainly contain $n\text{C}_2\text{S}-\text{C}_3\text{P}$, C_2S , RO, MgAl_2O_4 , and $\text{Ca}_3\text{Mg}(\text{SiO}_4)_2$. The P in slag mainly exists in the form of $n\text{C}_2\text{S}-\text{C}_3\text{P}$ solid solution. Besides, the intensities of characteristic peaks corresponding to $n\text{C}_2\text{S}-\text{C}_3\text{P}$ and C_2S gradually increase. This indicates that the increase of basicity is conducive to the formation of $n\text{C}_2\text{S}-\text{C}_3\text{P}$.

4.3. Analysis of Micro-Structure of Dephosphorization Slag by Raman Spectroscopy

Figure 8 shows the Raman spectra analysis results of Fe-rich phase in R155 slag, matrix phase C in R213 slag, and P-rich phases in R155 slag and R213 slag. In the figure, for example, R155-A represents the P-rich phase A in R155 slag. Because the P_2O_5 content in the

P-rich phases of R155 and R213 are obviously different, the embedded dephosphorization slag samples are used for the Raman spectrum analysis to study the micro-structures of these two P-rich phases. Besides, the micro-structures of Fe-rich phase B in R155 slag and matrix phase C in all slags are also characterized. Because the micro-structures of the matrix phases in all the slags are basically the same, the Raman analysis result of matrix phase in R213 slag is shown in Figure 8 as a representative result.

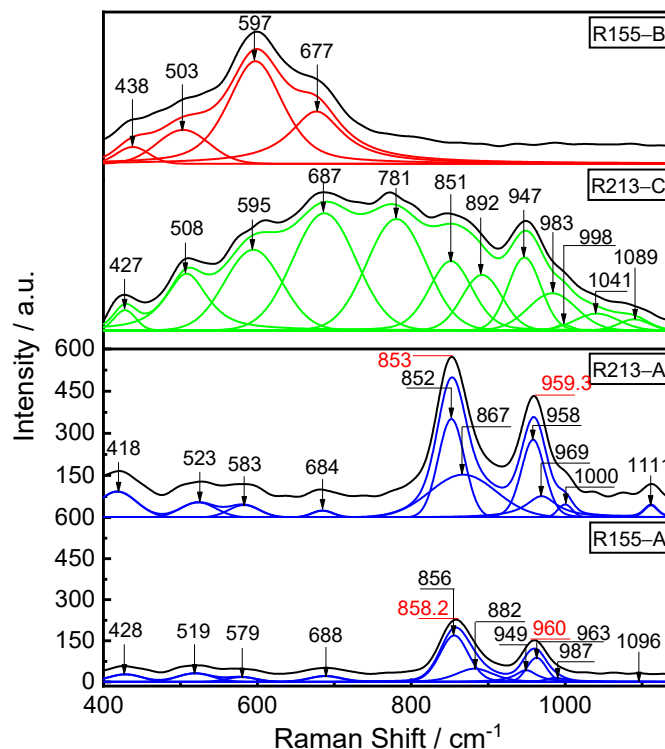


Figure 8. Raman spectra analysis of Fe-rich phase in R155 slag, matrix phase C in R213 slag, and P-rich phases in R155 slag and R213 slag.

All the original Raman spectra lines of the sample are first smoothed and then the corresponding baselines are subtracted as shown with the black lines in Figure 8. The fitting results of the corresponding Raman spectra are also shown in the figure with the red, green, and blue lines, which are fitted using the software peakfit v4.12. As shown in Figure 8, R155-B, it can be seen that the characteristic peaks of Fe-rich phase in dephosphorization slag are distributed in the low-frequency region from 400 to 800 cm^{-1} , and there is no obvious characteristic peak detected in the high-frequency region from 800 to 1200 cm^{-1} . A large envelope peak and a right shoulder peak appear near 597 cm^{-1} and 677 cm^{-1} , respectively, which correspond to $[\text{FeO}_6]$ -octahedron and $[\text{FeO}_4]$ -tetrahedron structure units [14,23]. In addition, the two weak peaks near 438 cm^{-1} and 503 cm^{-1} correspond to Si-O-Si and Si-O-Al bending vibration, respectively [24–27]. The results are consistent with the compositions of the Fe-rich phase in R155 in Table 4. This indicates that the Fe in the Fe-rich phase of dephosphorization slag mainly exists in the form of a network modifier with $[\text{FeO}_6]$ -octahedral structure, which is helpful in reducing the viscosity of slag. Because the compositions of RO phases in different dephosphorization slags with basicity above 1.55 are very close, the Raman analysis result of RO phases in R155 slag is shown in Figure 8 as a representative result.

The two strongest Raman peaks of P-rich phase in dephosphorization slag mainly appear in the high-frequency region, which are near 850 cm^{-1} and 960 cm^{-1} , respectively, as shown in Figure 8, R213-A and R155-A. In Table 4, the P-rich phase is mainly composed of $n\text{C}_2\text{S}-\text{C}_3\text{P}$ and a small amount of metal oxides. Therefore, it can be preliminarily judged

that the peaks in the high-frequency region are mainly the superposition of the peaks corresponding to $[\text{SiO}_4]$ -tetrahedron and $[\text{PO}_4]$ -tetrahedron.

In addition, from the black lines of R213-A and R155-A, the frequency shift phenomenon is found near the peaks of about 850 cm^{-1} . The peak positions corresponding to R213-A and R155-A are 853 cm^{-1} and 858.2 cm^{-1} , respectively, and the corresponding peak intensities decrease.

With the increase of the P_2O_5 content in the P-rich phase of R155-A and R213-A, the corresponding basicities of the P-rich phase are 2.55 and 3.58, respectively. The basicity of R213-A is obviously higher, so it is easy to increase the structural units with low bridging oxygen number in the P-rich phase. Therefore, there are far more free CaO ions in the phase region, which is helpful for reducing the polymerization degree of $n\text{C}_2\text{S}-\text{C}_3\text{P}$. This will further cause the interaction between the micro-structure units to decrease, which results in the decrease of the vibration frequency.

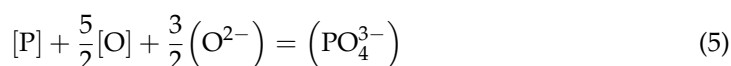
Because the experimental conditions of Raman analysis for P-rich phases in R213 and R155 are the same, the intensities of Raman signals of the different structural units can be used to compare the contents of the corresponding structural units. From the fitting peaks of the P-rich phase, it can be seen that the Raman intensities of the corresponding P-O-Ca and P-O-Si structural units in R213-A are significantly higher than those in R155-A. This indicates that the mole fractions of P-O-Ca and P-O-Si structural units in the P-rich phase in dephosphorization slag of R213 are obviously higher. According to the results by Zheng et al. [28], the area fractions of P-O-Ca and P-O-Si units can be calculated for comparing mole fractions. The area fractions of P-O-Ca and P-O-Si units in the high-frequency region in R213-A are 22.6% and 2.59%, respectively, which are higher than those in R155-A of 13.2% and 0.02%. The results are consistent with the results of the corresponding Raman signal intensities of P-O-Ca and P-O-Si units. The value of coefficient n of the $n\text{C}_2\text{S}-\text{C}_3\text{P}$ in R213-A is smaller than that in R155-A. In addition, the Raman intensity of the P-O-Ca structure unit in the P-rich phase is significantly higher than that of the P-O-Si structure unit, indicating that most of the phosphorus in P-rich phase exists in the P-O-Ca structure unit along with a small amount of phosphorus in the P-O-Si structure unit. The structural units corresponding to the fitting peaks in the Raman spectrum are shown in Table 5. The i in Q^i is the number of bridging oxygen per silicon atom.

Table 5. Structure units corresponding to the fitting peaks in Raman spectra.

Sample	R155-A	R213-A	R213-C	R155-B	Raman Assignments
Raman shift (cm^{-1})	428	418	428	438	Si-O-Si [24,25]
	519	523	508	503	Si-O-Al [26,27]
	579	583	595	597	$[\text{FeO}_6]$ [23,29–31]
	688	684	687	677	$[\text{FeO}_4]$ [23,29–31]
			781		$[\text{AlO}_4]$ [23,29–31]
	856	852	851		Q^0 [32]
	882	867	892		Q^1 [32]
	983	969	983		Q^2 [32]
			1041		Q^3 [32]
	949	958	947		P-O-Ca [13]
	987	1000	998		P-O-P [33]
1096	1111	1089		P-O-Si [13,33]	

4.4. Effect of Basicity on Activity Coefficient of P_2O_5 and the Basicity in the Matrix Phase of Dephosphorization Slag

The ion reaction equation of dephosphorization of hot metal can be expressed as Equation (5). It can be seen that the dephosphorization can be promoted by increasing the activities of $[\text{O}]$ and (CaO) .



It was found that the dephosphorization ratio in the hot metal can reach the maximum value approximately when the reaction time is 15 min [18]. Therefore, when the dephosphorization reaction of hot metal is assumed to be in a quasi-equilibrium state, the activity of P_2O_5 , $\alpha_{(P_2O_5)}$, and activity coefficient of P_2O_5 , $\gamma_{(P_2O_5)}$, in the liquid slag phase of the CaO-SiO₂-FeO-P₂O₅-Al₂O₃-MnO-MgO slag system can be calculated by the regular solution model. The main reason for selecting this model is that it does not involve the structure problem of silicon-oxygen complex-ion whose real structure has not been fully understood. In this model, the cations such as Ca²⁺, Fe²⁺, Fe³⁺, Si⁴⁺, Al³⁺, and P⁵⁺ are randomly distributed in the matrix phase of slag containing oxygenated anions, which are the common anions of various cations. The activity coefficient of component i , $\gamma_{i(R.S.)}$, in a multi-component regular solution can be expressed in Equation (6). This is based on the interaction energy between cations, α_{ij} , obtained by Ban—ya, as shown in Table 6 [34]. The $\gamma_{(P_2O_5)}$ and $\alpha_{(P_2O_5)}$ can be represented by Equations (7)–(9).

$$RT \ln \gamma_{i(R.S.)} = \sum_j \alpha_{ij} X_j^2 + \sum_j \sum_k (\alpha_{ij} + \alpha_{ik} + \alpha_{jk}) X_j X_k \quad (6)$$

$$\begin{aligned} RT \ln \gamma_{PO_{2.5}(R.S.)} = & -31380X_{FeO}^2 - 84940X_{MnO}^2 - 251040X_{CaO}^2 - 37660X_{MgO}^2 + 83680X_{SiO_2}^2 \\ & - 261500X_{Al_2O_3}^2 - 123430X_{FeO}X_{MnO} - 251040X_{FeO}X_{CaO} - 102510X_{FeO}X_{MgO} \\ & + 94140X_{FeO}X_{SiO_2} - 251880X_{FeO}X_{Al_2O_3} - 243930X_{MnO}X_{CaO} - 184520X_{MnO}X_{MgO} \\ & + 74050X_{MnO}X_{SiO_2} - 305440X_{MnO}X_{Al_2O_3} - 156070X_{CaO}X_{MgO} + 94140X_{CaO}X_{SiO_2} \\ & - 262760X_{CaO}X_{Al_2O_3} + 112960X_{MgO}X_{SiO_2} - 228030X_{MgO}X_{Al_2O_3} - 50210X_{SiO_2}X_{Al_2O_3} \quad (J) \end{aligned} \quad (7)$$

$$RT \ln \alpha_{P_2O_5(L)} = 2RT \ln \alpha_{PO_{2.5}(R.S.)} + 52720 - 230.706T(J) \quad (8)$$

The $\gamma_{(P_2O_5)}$ in the liquid phase is represented by Equation (9).

$$\gamma_{(P_2O_5)} = \frac{a_{P_2O_5(L)}}{X_{(P_2O_5)}} \quad (9)$$

where X_{MO} represents the mole fraction of MO in the matrix phase C at different basicities as shown in Table 4. R is the ideal gas constant with a value of 8.314 J·mol⁻¹·k⁻¹. T is the corresponding dephosphorization temperature.

Table 6. Interaction energy between cations of major components in steelmaking slag, α_{ij} . (J).

i	j	Fe ²⁺	Fe ³⁺	Mn ²⁺	Ca ²⁺	Mg ²⁺	Si ⁴⁺	P ⁵⁺	Al ³⁺
Fe ²⁺	—	—	−18,660	7110	−31,380	33,470	−41,840	−31,380	−41,000
Fe ³⁺	−18,660	—	−56,480	−95,810	−2930	32,640	14,640	−161,080	−161,080
Mn ²⁺	7110	−56,480	—	−92,050	61,920	−75,310	−84,940	−83,680	−83,680
Ca ²⁺	−31,380	−95,810	−92,050	—	−100,420	−133,890	−251,040	−154,810	−154,810
Mg ²⁺	33,470	−2930	61,920	−100,420	—	−66,940	−37,660	−71,130	−71,130
Si ⁴⁺	−41,840	32,640	−75,310	−133,890	−66,940	—	83,680	−127,610	−127,610
P ⁵⁺	−31,380	14,640	−84,940	−251,040	−37,660	83,680	—	−261,500	−261,500
Al ³⁺	−41,000	−161,080	−83,680	−154,810	−71,130	−127,610	−261,500	—	—

The conversion from $\alpha_{PO_{2.5}(R.S.)}$ to $\alpha_{P_2O_5(L)}$ is shown in Equation (8), where the subscript indicates the reference state of the activity. (R.S.) indicates the pure PO_{2.5} liquid under the assumption that it is the regular solution and (L) represents the pure P₂O₅ liquid.

Figure 9 shows the effect of the basicity of the dephosphorization slag on the $\gamma_{(P_2O_5)}$ and basicity in the liquid phase. With the increase of the basicity of the dephosphorization slag, the $\gamma_{(P_2O_5)}$ in the liquid phase decreases, while the basicity in the liquid phase increases.

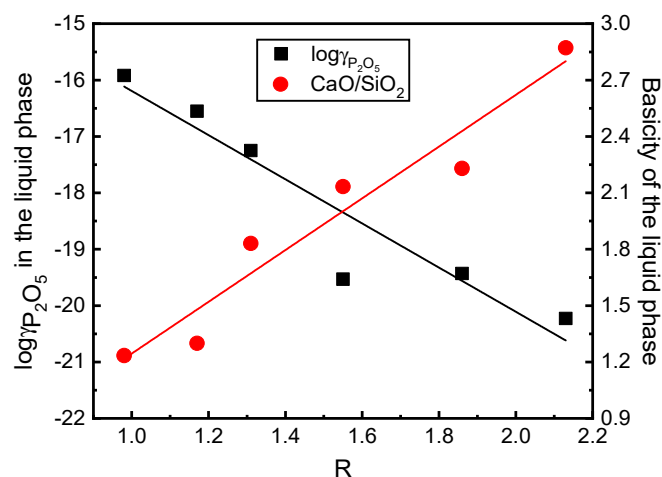


Figure 9. Effect of the basicity of the dephosphorization slag on the $\gamma_{(P_2O_5)}$ and basicity in the liquid phase.

At the basicities from 0.98 to 1.31, the CaO in slag mainly exists in the liquid phase, as shown in Figures 5 and 6. Therefore, with the increase of the basicity of dephosphorization slag, the amount of CaO in the slag increases, which results in the increase of the CaO content in the liquid phase. As the amount of SiO₂ is basically unchanged, therefore the basicity in the liquid phase will increase.

At the basicities from 1.55 to 2.13, the CaO and SiO₂ in slag are distributed in both P-rich phase and matrix phase at the same time, and the change is relatively complex. The specific reasons for the change of the basicity in the liquid phase need to be further studied.

From Equation (7), it can be found that the $\gamma_{(P_2O_5)}$ values decrease with the increase of CaO, FeO, and Al₂O₃ contents, but increase with the increase of SiO₂ content at the same temperature. According to the compositions of matrix phase C in Table 4, with the increase of the basicity of dephosphorization slag, the FeO and Al₂O₃ contents increase, the SiO₂ content decreases, and the CaO content increases first and then changes slightly. Therefore, the $\gamma_{(P_2O_5)}$ values mainly decrease with the increase of the basicity of dephosphorization slag. From the view of thermodynamics, the decrease of the $\gamma_{(P_2O_5)}$ in the liquid phase will promote the P in hot metal to be oxidized to P₂O₅ and improve the dephosphorization ratio of hot metal.

5. Conclusions

In the present work, the effect of the basicity at the lower range from 0.98 to 2.13 on dephosphorization of hot metal with CaO-FeO-SiO₂-MnO-MgO-Al₂O₃ slag at 1623 K was studied through high-temperature laboratorial experiments. The following conclusions can be obtained.

- (1) With the increase of the basicity from 0.98 to 1.31, the P and C contents in hot metal rapidly decrease and increase at first, respectively. With the increase of the basicity from 1.31 to 2.13, the P and C contents gradually decrease and increase, respectively. With the increase of the basicity, the Mn contents in the hot metal increase gradually. In the slag, the MnO content decreases gradually, and the P₂O₅ content in slag only increases slightly. The T.Fe content firstly decreases and then increases slightly.
- (2) From the SEM-EDS and XRD results, when the basicities are 0.98 and 1.17, the slag is mainly composed of matrix phase rich in P, Fe₂SiO₄ phase, and spinel phase rich in Al, Mg, Fe, and Mn. With the increase of the basicity to 1.31, the slag is mainly composed of matrix phase and a small amount of pure iron. With the increase of the basicity to 1.55 and 1.86, the slag is mainly composed of P-rich phase containing nC₂S-C₃P solid solution, Fe-rich phase, and matrix phase. With further increase of the basicity to 2.13, the slag is mainly composed of P-rich phase and matrix phase.

- (3) With the increase of the basicity, the phase containing the high P content changes from the matrix phase into the P-rich phase. Therefore, under the present experimental conditions, the P-rich phase can only be precipitated from the liquid slag when the basicity is higher than 1.55, which is a benefit to the dephosphorization.
- (4) The Raman intensity of the P-O-Ca structure unit in the P-rich phase is significantly higher than that of the P-O-Si structure unit, indicating that most of the phosphorus in P-rich phase exists in the P-O-Ca structure unit along with a small amount of phosphorus in the P-O-Si structure unit.
- (5) With the increase of the basicity of the dephosphorization slag, the activity coefficient of P_2O_5 , $\gamma_{(P_2O_5)}$, in the liquid phase decreases, while the basicity in the liquid phase increases.

Author Contributions: Conceptualization, W.Y. and J.Y.; methodology, J.Y.; validation, Y.Q.; formal analysis, W.Y.; investigation, W.Y.; resources, Y.Q.; data curation, R.Z. and H.S.; writing—original draft preparation, W.Y.; writing—review and editing, J.Y.; visualization, W.Y.; supervision, J.Y.; project administration, J.Y.; funding acquisition, J.Y. All authors have read and agreed to the published version of the manuscript.

Funding: This work is financially supported by the National Natural Science Foundation of China (Grant No. U1960202).

Institutional Review Board Statement: The study did not involve humans or animals.

Informed Consent Statement: The study did not involve humans or animals.

Data Availability Statement: Data supporting reported results can be found in this paper.

Conflicts of Interest: The authors declare no conflict of interest.

References

1. Ogawa, Y.; Yano, M.; Kitamura, S.; Hirata, H. Development of the continuous dephosphorization and decarburization process using BOF. *Tetsu-to-Hagané* **2001**, *87*, 21–28. [[CrossRef](#)]
2. Fix, W.; Heymann, H.; Heinke, R. Subsolidus relations in the system $2CaO \cdot SiO_2 - 3CaO \cdot P_2O_5$. *J. Am. Ceram. Soc.* **1969**, *52*, 346–347. [[CrossRef](#)]
3. Zhao, B.; Wu, W.; Wu, W.; Meng, H.; Gao, Q.; Guo, Z. Study on the occurrence of phosphorus in the slag of hot metal dephosphorization for stainless steel production. *Steel Res. Int.* **2020**, *91*, 2000021. [[CrossRef](#)]
4. Zhou, J.; Bi, X.; Yue, R.; Yang, F. Phosphorus distribution ratio between multi phase $CaO-FeO_t-SiO_2-P_2O_5$ (6%–13%) slags with MP near hot metal temperature and C-saturated molten iron at 1 573 K. *ISIJ Int.* **2017**, *57*, 706–712. [[CrossRef](#)]
5. Kitamura, S.Y.; Yonezawa, K.; Ogawa, Y.; Sasaki, N. Improvement of reaction efficiency in hot metal dephosphorisation. *Ironmak. Steelmak.* **2002**, *29*, 121–124. [[CrossRef](#)]
6. Liu, F.; Wang, G.; Zhao, Y.; Tan, J.; Zhao, C.; Wang, Q. Hot metal dephosphorisation by low basicity slag in the early stage of converting process. *Ironmak. Steelmak.* **2019**, *46*, 392–403. [[CrossRef](#)]
7. Suzuki, M.; Nakano, S.; Serizawa, H.; Umesaki, N. In-situ phase identification of crystallized compound from $2CaO \cdot SiO_2 - 3CaO \cdot P_2O_5$ liquid. *ISIJ Int.* **2020**, *60*, 1127–1134. [[CrossRef](#)]
8. Shu, Q.F.; Liu, Y. Effects of basicity, MgO and MnO on mineralogical phases of $CaO-FeO_x-SiO_2-P_2O_5$ slag. *Ironmak. Steelmak.* **2017**, *45*, 363–370. [[CrossRef](#)]
9. Lin, Y.; Liu, Y.; Chou, K.; Shu, Q. Effects of oxygen atmosphere, FeO_x and basicity on mineralogical phases of $CaO-SiO_2-MgO-Al_2O_3-Fe_tO-P_2O_5$ steelmaking slag. *Ironmak. Steelmak.* **2019**, *46*, 987–997. [[CrossRef](#)]
10. Uchida, Y.I.; Sasaki, N.; Miki, Y. Change of phosphorus-concentrated phase in low basicity steelmaking slag. *ISIJ Int.* **2018**, *58*, 869–875. [[CrossRef](#)]
11. Ye, G.F.; Yang, J.; Zhang, R.H.; Yang, W.K.; Sun, H. Behavior of phosphorus enrichment in dephosphorization slag at low temperature and low basicity. *Int. J. Min. Met. Mater.* **2021**, *28*, 66–75. [[CrossRef](#)]
12. Yang, W.K.; Yang, J.; Zhang, R.H.; Sun, H. Effect of the initial P content on dephosphorization of hot metal with low basicity slag at 1623 K. *Steel Res. Int.* **2021**, *92*, 2100066. [[CrossRef](#)]
13. Wang, Z.; Cai, S.; Zhang, M.; Guo, M.; Zhang, Z. Structural investigation of phosphorus in $CaO-SiO_2-P_2O_5$ ternary glass. *Metall. Mater. Trans. B* **2017**, *48*, 1139–1148. [[CrossRef](#)]
14. Wang, Z.J.; Shu, Q.F.; Sridhar, S.; Zhang, M.; Guo, M.; Zhang, Z.T. Effect of P_2O_5 and Fe_tO on the viscosity and slag structure in steelmaking slags. *Metall. Mater. Trans. B* **2015**, *46*, 758–765. [[CrossRef](#)]

15. Yang, W.K.; Yang, J.; Shi, Y.Q.; Yang, Z.J.; Gao, F.B.; Zhang, R.H.; Ye, G.F. Effect of temperature on dephosphorization of hot metal in double slag converter steelmaking process by high-temperature laboratorial experiments. *Steel Res. Int.* **2021**, *92*, 2000438. [[CrossRef](#)]
16. Yang, W.K.; Yang, J.; Shi, Y.Q.; Yang, Z.J.; Gao, F.B.; Zhang, R.H.; Sun, H. Effect of the Fe_2O_3 addition amount on dephosphorization of hot metal with low basicity slag by high-temperature laboratorial experiments. *Metals* **2021**, *11*, 417. [[CrossRef](#)]
17. Yang, W.K.; Yang, J.; Zhang, R.H.; Sun, H. Microstructure and viscosity of dephosphorization slag in new double slag converter steelmaking process. *ISIJ Int.* **2021**, *61*. [[CrossRef](#)]
18. Xia, Y.; Li, J.; Fan, D.; Hou, G. Effects of interfacial oxygen potential and slag phase changing during slag formation process on dephosphorization behavior. *ISIJ Int.* **2019**, *59*, 1519–1526. [[CrossRef](#)]
19. Yang, W.K.; Yang, J.; Shi, Y.Q.; Yang, Z.J.; Gao, F.B.; Zhang, R.H.; Ye, G.F. Effect of basicity on dephosphorization of hot metal with a low basicity slag at 1653 K. *Ironmak. Steelmak.* **2021**, *48*, 69–77. [[CrossRef](#)]
20. Zhu, C.Y.; Li, G.Q.; Chen, Z.P.; Ma, G.J.; Liu, J. Manganese distribution equilibrium between $\text{CaO-Fe}_t\text{O-SiO}_2\text{-MnO-P}_2\text{O}_5\text{-(Al}_2\text{O}_3)$ slags and carbon saturated iron. *ISIJ Int.* **2008**, *48*, 123–129. [[CrossRef](#)]
21. Yang, W.K.; Zhang, R.H.; Sun, H.; Yang, J. Dephosphorization in new double slag converter steelmaking process with high temperature laboratorial experiments. *Steel Res. Int.* **2021**. [[CrossRef](#)]
22. Suito, H.; Inoue, R. Thermodynamic assessment of hot metal and steel dephosphorization with MnO-containing BOF slags. *ISIJ Int.* **1995**, *35*, 258–265. [[CrossRef](#)]
23. Jung, S.S.; Sohn, I. Crystallization control for remediation of an $\text{Fe}_t\text{O-rich CaO-SiO}_2\text{-Al}_2\text{O}_3\text{-MgO}$ EAF waste slag. *Environ. Sci. Technol.* **2014**, *48*, 1886–1892. [[CrossRef](#)]
24. Hass, M. Raman spectra of vitreous silica, germania and sodium silicate glasses. *J. Phys. Chem. Solids.* **1970**, *31*, 415–422. [[CrossRef](#)]
25. Agathopoulos, S.; Tulyaganov, D.; Ventura, J.; Kannan, S.; Saranti, A.; Karakassides, M.; Ferreira, J. Structural analysis and devitrification of glasses based on the CaO-MgO-SiO_2 system with B_2O_3 , Na_2O , CaF_2 and P_2O_5 additives. *J. Non-Cryst. Solids.* **2006**, *352*, 322–328. [[CrossRef](#)]
26. McKeown, D.; Galeener, F.; Brown, G., Jr. Raman studies of Al coordination in silica-rich sodium aluminosilicate glasses and some related minerals. *J. Non-Cryst. Solids.* **1984**, *68*, 361–378. [[CrossRef](#)]
27. Mohri, M.; Sasaki, Y.; Ishii, K. Comparative roles of Al^{3+} and Fe^{3+} ions for network construction in sodium silicate melts. *ISIJ Int.* **2001**, *41*, 410–415. [[CrossRef](#)]
28. Zheng, K.; Zhang, Z.; Liu, L.; Wang, X. Investigation of the viscosity and structural properties of $\text{CaO-SiO}_2\text{-TiO}_2$ slags. *Metall. Mater. Trans. B* **2014**, *45*, 1389–1397. [[CrossRef](#)]
29. Tarte, P. Infra-red spectra of inorganic aluminates and characteristic vibrational frequencies of AlO_4 tetrahedra and AlO_6 octahedra. *Spectrochim. Acta Part A: Mol. Spectrosc.* **1967**, *23*, 2127–2143. [[CrossRef](#)]
30. Leekes, G.; Nowack, N.; Schlegelmilch, F. Dissolution of water vapour in ESR-slugs of the systems $\text{CaO-Al}_2\text{O}_3$ and $\text{CaF}_2\text{-CaO-Al}_2\text{O}_3$ by application of Fourier-Transform-Infrared-Spectroscopy. *Steel Res.* **1988**, *59*, 406–416. [[CrossRef](#)]
31. Park, J.H.; Min, D.J.; Song, H.S. Structural investigation of $\text{CaO-Al}_2\text{O}_3$ and $\text{CaO-Al}_2\text{O}_3\text{-CaF}_2$ slags via Fourier transform infrared spectra. *ISIJ Int.* **2002**, *42*, 38–43. [[CrossRef](#)]
32. Mysen, B.O.; Ryerson, F.J.; Virgo, D. The structural role of phosphorus in silicate melts. *Am. Mineral.* **1981**, *66*, 106–117.
33. Wong, J. Vibrational spectra of vapor-deposited binary phosphosilicate glasses. *J. Non-Cryst. Solids* **1976**, *20*, 83–100. [[CrossRef](#)]
34. Ban, Y.S. Mathematical expression of slag-metal reactions in steelmaking process by quadratic formalism based on the regular solution model. *ISIJ Int.* **1993**, *33*, 2–11. [[CrossRef](#)]